ARCHIVE OF MECHANICAL ENGINEERING

DOI: 10.24425/ame.2022.143097 2022, Vol. 69, No. 4, pp. 645–666

Jerzy SAWICKI [1], Tomasz PACZKOWSKI [2], Jarosław ZDROJEWSKI [3]

Analysis of the effect of inertial forces of the electrolyte flow on the ECM machining effects of curvilinear rotary surfaces

Received 29 November 2021, **Revised** 1 July 2022, **Accepted** 20 July 2022, **Published online** 30 November 2022

Keywords: centrifugal forces, longitudinal forces, electrochemical machining, electrolyte flow, computer simulation, method of perturbation

This paper presents an analysis of the impact of inertial forces of the electrolyte flow in an interelectrode gap on the effects of ECM process of curvilinear rotary surfaces. Considering a laminar flow in the interelectrode gap, the equations of the flow of the mixture of electrolyte and hydrogen in the curvilinear orthogonal coordinate system have been defined. Two classes of equations of motion have been formulated, which differ in the estimates referred to the components of velocity and pressure, and which were analytically solved using the method of perturbation.

Using the machined surface shape evolution equation, the energy equation, and the analytical solutions for velocity and pressure, the ECM-characteristic distributions have been determined: of mean velocity, pressure, mean temperature, current density, gas phase concentration, the gap height after the set machining time for the case when there is no influence of inertial forces, the effect of centrifugal forces and, at the same time, centrifugal and longitudinal inertial forces.

✉ Jerzy Sawicki, e-mail: jerzy.sawicki@pbs.edu.pl

[1]Department of Mechanics and Computer Methods, Bydgoszcz University of Science and Technology,Bydgoszcz, Poland. ORCID: 0000-0001-8842-1034

[2]Department of Manufacturing Techniques, Bydgoszcz University of Science and Technology, Bydgoszcz, Poland. ORCID: 0000-0003-2861-8817

[3]Department of Digital Technology, Bydgoszcz University of Science and Technology, Bydgoszcz, Poland. ORCID: 0000-0001-7652-4685

1. Introduction

Electrochemical Machining (ECM) is an effective method of machining complex-shaped parts made of hard-to-cut materials, e.g., turbojet engine blades, steam turbine blades, turbine and turbopump discs, dies, punches, especially from sintered carbides, surgical implants, artillery shells, etc. [1, 2]. ECM, besides the electroerosion machining (EDM), is every so often the only method of processing for macro, micro and nano complex-shape elements that are made from difficult to process materials [3]. This machining is also widely used for making holes [4]. Electrochemical micromachining seems to be a highly promising technique in many application areas, especially in the electronics industry of the future [5].

In electrochemical machining, a material is shaped using anode dissolution. In general, machining involves the ECM workpiece (WP) machining with a positive electrode (anode) and, a tool electrode (TE) with a negative electrode (cathode). The gap between the anode and the cathode is filled with an electrically conducting solution (electrolyte). The flow of the current between the electrodes triggers a process of anode dissolution, resulting in material removal from the anode (WP). In electrochemical machining, one can create conditions which allow for high performance process and surface smoothness through selecting appropriate machining parameters and materials for the anode, the cathode, and the electrolyte [6–8].

Electrochemical machining is often considered to be a finishing touch and is used to improve the macro- and microgeometry of parts and elements preliminarily processed by other methods [9, 10]. The paper [11] presents a comprehensive process of electrochemical unidirectional longitudinal honing as a finishing process. Experimental studies confirming the improvement of macro and microgeometry of holes in comparison to the classical machining of large holes were carried out on a machine tool constructed by the author's team. The authors of another paper [12] point to the influence of hydrodynamic instability on the topography of the workpiece surface. The combination of electrochemical milling with electrochemical grinding allowed to increase the efficiency of the finishing process [13, 14].

A variable field of velocity, pressure, temperature, current density, the concentration of gases which appear in the interelectrode gap (IEG) and chemical reactions and electrode processes all contribute to electrochemical dissolution that results in a change of the shape and the dimensions of a WP in the ECM process. The complex physicochemical processes which occur in the IEG and an often-complex shape of the machined surfaces make the ECM process three-dimensional. Interestingly, in most cases the 3D problem is either simplified to ECM process being considered as a single- or possibly two-dimensional process. With such ECM process models, the TE shape and then the shape of the TE in the input plane (of the cross-section) are determined. Assuming that the WP is a spaciously complex piece, going to successive cross-sections determining the one-dimensional – or sometimes two-dimensional – machining field, the phenomena accompanying third dimension are

disregarded on purpose. It usually leads to significant errors of such simulations. As a result, it is necessary to introduce TE designing corrections that are prolonging the ECM process and, consequently, lowering the performance of the process of electrochemical dissolution.

In addition to the ideal ECM model, laminar and turbulent flow of electrolyte in the IEG is considered in [15–22].

In the ECM continuous machining process, the TE usually makes a translational motion towards the WP. Kinematically, the machining process can be complex – a vibrating electrode, an electrode performing a rotational motion, etc. The electrolyte fed to the IEG – indispensable for the dissolution process – also discharges products from the interelectrode space (molecules of hydrogen and digested metal ions). In the IEG, there is a thermodynamically complex multiphase flow of molecules of hydrogen, digested metal, and the carrier, namely electrolyte [17, 18].

The properties of the electrolyte and hydrodynamic parameters of the electrolyte flow affect the processes of the mass, momentum, and energy transfer in the IEG. It is thus essential to ascertain that the machining parameters are correct to prevent the occurrence of cavitation zones, a critical flow, an excessive increase in the temperature of electrolyte, or an excessively high volumetric concentration of the gas phase [19, 20, 22].

The essence of the ECM mathematical modeling is determining the evolution of the shape of the WP surface in time and the distribution of the physicochemical conditions found in the machining area, including: the distribution of the IEG height, the electrolyte flow rate, static pressure, current density, temperature, and the volumetric concentration of the gas phase [23–27].

The modeling and simulation of the ECM process for surfaces with a curvilinear contour and curvilinear rotating surfaces, including the processes of hole machining, milling, and grinding, are described in numerous works. One paper [11] presents the process of electrochemical machining of curved surfaces based on a one-dimensional model of electrolyte flow in the inter-electrode gap. Similarly, another paper [17] presents physical and mathematical models based mainly on one-dimensional electrolyte flow, used to develop a simulation program working as an ECM computer aided system (CAE-ECM). Several examples of the CAE-ECM system use were discussed. The papers [18, 25, 26] present selected topics of the ECM machining for curvilinear rotating surfaces. Based on the principles of mass, momentum, and energy conservation, two-dimensional equations were formulated for the inter-electrode gap flow of the electrolyte and hydrogen mixture. Computer simulations for various electrode-workpiece kinematic systems were carried out, discussing the distribution of electrolyte velocity, pressure, temperature, current density, gas phase volume concentration, and the thickness of post-machining gap. One paper [27] presents a mathematical model of electrochemical machining for two-dimensional curved surfaces with the use of

matrix equations that were solved numerically. Another paper [20] also presents the impact of hydrodynamic conditions of electrolyte flow on analysis of critical parameters related to ECM machining of curved rotational surfaces. Three papers [28–30] concern hole electrochemical machining and examine the influence of electrolyte conductivity on tool wear. In one of these papers [29] CFD computer simulations were used to determine selected machining parameters that improve the machining accuracy of the cooling holes in a turbine blade. The paper [30] presents an innovative method of ECM for machining holes based on an electrode with a gradually decreasing conductive surface. The process was modeled to study the electric potential and the current density distribution at the electrode surface. In [31] a suitable method of electrolyte feeding was proposed to eliminate electrolyte flow traces on aircraft engine blades. The flow view was obtained using the finite element method. The simulation results were confirmed by an experiment.

Noteworthy are monographs [11, 32, 33], in which the basics of theoretical electrochemical machining are presented.

One paper [11] provides an analysis of the ECM for the axisymmetric shaped surface based on an approximate one-dimensional flow model applied for the two-dimensional problem – the axisymmetric flow. The analysis has provided the values for the distribution of static pressure, mean velocity, temperature, gas phase concentration and the IEG thickness. The second paper [21] considers a process based on the ideal ECM model, with a segment rotating and vibrating electrode. Another paper [24] provides an analysis of ECM axisymmetric surface machining, considering the real conditions in the IEG. Using the shape evolution equation, the distribution of the IEG thickness after machining and physical parameters of the ECM process for respective cases of movement of the electrodes limiting the flow of electrolyte in the gap are determined.

This paper is an attempt to analyze the impact of the inertial forces of electrolyte flow in laminar flow conditions on the effects of the ECM process of curvilinear rotary surfaces. The aim is to determine the distribution of the IEG height, the electrolyte flow rate, temperature, static pressure, current density, and the volumetric concentration of the gas phase dependent on the effect of electrolyte flow inertia in the IEG.

2. ECM machining process modeling

2.1. Workpiece shape evolution equation

In a $R\theta Z$ cylindrical coordinate system related to a fixed anode (WP) (Fig. 1) the rotating surface equation is as follows:

$$Z = Z_A(R, t). \tag{1}$$

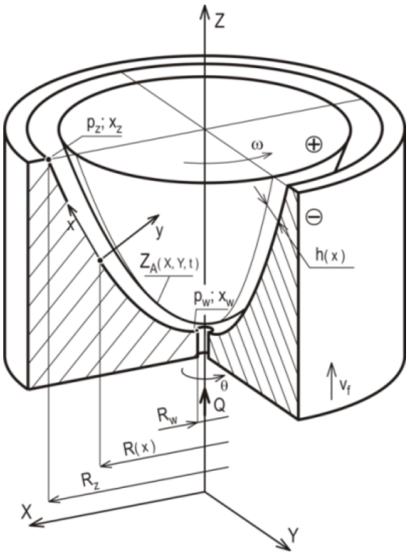

Fig. 1. Interelectrode gap

The shape of evolution equation for the machined surface assumes the following form [20, 23, 25, 26]:

$$\frac{\partial Z_A}{\partial t} = k_V j_A \sqrt{1 + \left(\frac{\partial Z_A}{\partial R}\right)^2} \quad \text{for } t = 0, \quad Z_A = Z_A(R), \tag{2}$$

where: k_V – is the coefficient electrochemical machinability which is defined as the volume of material dissolved per unit electrical charge and $Z_A(R)$ describes an initial shape of the WP surface.

Assuming that the distribution of the potential along the normal section to the TE is linear, as is often assumed for the technology process calculations, the function of the current density is presented with the following formula [17, 23]:

$$j_A = \varkappa_0 \Phi_{\mathrm{TG}}^{-1} \frac{U - E}{h}, \tag{3}$$

where: κ_0 – the electrolyte conductivity at T_0 and $\beta = 0$, T_0 – the initial temperature of the electrolyte, h – the lowest IEG thickness, β – the void fraction (volumetric gas concentration), U – the working voltage between the TE cathode and WP anode, E – the total overpotential at the inlet of the gap.

Let us assume that the electrochemical machining surfaces of the TE and the WP are similar in terms of geometry, which gives us a two-phase electrolyte-hydrogen zone filling the gap completely. The volumetric concentration of the gas phase changes along the Φ_{TG} flow and function, describing the effect of temperature and gas-phase concentration on the conductivity of the mixture in the IEG in the

following form [17, 18, 23, 26]:

$$\Phi_{\mathrm{TG}} = \frac{1}{h}\left[\int_0^h \frac{\mathrm{d}y}{(1+\alpha_T \Delta T)\,(1-\beta)^{\frac{3}{2}}}\right], \tag{4}$$

where: α_T – conductivity coefficient of the electrolyte at T, $\Delta T = T - T_0$ – temperature increment.

2.2. Equations of motion of the electrolyte and hydrogen in the curvilinear coordinate system

System of equations (2)–(4) is not a closed system. To close the system of equations, it is indispensable to determine the temperature distribution in the IEG thickness (h) and the gas phase concentration (β). Determining the temperature distribution in the IEG requires an analysis of the flow of the mixture of electrolyte and hydrogen in the gap.

The flow equations of the electrolyte and hydrogen mixture in the locally orthogonal curvilinear coordinate system $x\theta y$ assume the following forms [26]:

– mixture flow continuity equations:

for electrolyte:

$$\frac{1}{R}\frac{\partial\left(\rho_e R v_x\right)}{\partial x} + \frac{1}{R}\frac{\partial\left(\rho_e v_\theta\right)}{\partial \theta} + \frac{\partial\left(\rho_e v_y\right)}{\partial y} = 0; \tag{5}$$

for hydrogen:

$$\frac{1}{R}\frac{\partial\left(\rho_H R v_x\right)}{\partial x} + \frac{1}{R}\frac{\partial\left(\rho_H v_\theta\right)}{\partial \theta} + \frac{\partial\left(\rho_H v_y\right)}{\partial y} = j\eta_H k_H h^{-1} \tag{6}$$

momentum equation:

$$\begin{aligned}\rho_e\left(v_x\frac{\partial v_x}{\partial x} + \frac{v_\theta}{R}\frac{\partial v_x}{\partial \theta} + v_y\frac{\partial v_x}{\partial y} - v_\theta^2\frac{R'}{R}\right) &= -\frac{\partial p}{\partial x} + \frac{1}{R}\frac{\partial}{\partial x}\mu\left\{2R\frac{\partial v_x}{\partial x}\right.\\ &-\frac{2}{3}\left[\frac{1}{R}\frac{\partial\left(R v_x\right)}{\partial x} + \frac{1}{R}\frac{\partial v_\theta}{\partial \theta} + \frac{\partial v_y}{\partial y}\right]\Bigg\} + \frac{1}{R}\frac{\partial}{\partial \theta}\mu\left[\left(\frac{1}{R}\frac{\partial v_x}{\partial \theta} + \frac{\partial v_\theta}{\partial x} - v_\theta\frac{R'}{R}\right)\right.\\ &\left.-2\left(\frac{1}{R}\frac{\partial v_\theta}{\partial \theta} + v_x\frac{R'}{R}\right)\right] + \frac{\partial}{\partial y}\mu\left(\frac{\partial v_y}{\partial x} + \frac{\partial v_x}{\partial y}\right),\end{aligned} \tag{7}$$

$$\begin{aligned}\rho_e\left(v_x\frac{\partial v_\theta}{\partial x} + \frac{v_\theta}{R}\frac{\partial v_\theta}{\partial \theta} + v_y\frac{\partial v_\theta}{\partial y} + v_x v_\theta\frac{R'}{R}\right) &= -\frac{1}{R}\frac{\partial p}{\partial \theta}\\ &+\frac{1}{R}\frac{\partial}{\partial x}R^2\mu\left(\frac{1}{R}\frac{\partial v_x}{\partial \theta} + \frac{\partial v_\theta}{\partial x} + -v_\theta\frac{R'}{R}\right) + \frac{1}{R}\frac{\partial}{\partial \theta}\mu\left\{\left(\frac{1}{R}\frac{\partial v_\theta}{\partial \theta} + v_x\frac{R'}{R}\right)\right.\\ &\left.-\frac{2}{3}\left[\frac{1}{R}\frac{\partial\left(R v_x\right)}{\partial x} + \frac{1}{R}\frac{\partial v_\theta}{\partial \theta} + \frac{\partial v_y}{\partial y}\right]\right\} + \frac{\partial}{\partial y}\mu\left(\frac{1}{R}\frac{\partial v_y}{\partial \theta} + \frac{\partial v_\theta}{\partial y}\right),\end{aligned} \tag{8}$$

$$\rho_e\left(v_x\frac{\partial v_y}{\partial x}+\frac{v_\theta}{R}\frac{\partial v_y}{\partial \theta}+v_y\frac{\partial v_y}{\partial y}\right)= -\frac{\partial p}{\partial y}+\frac{1}{R}\frac{\partial}{\partial x}R\mu\left(\frac{1}{R}\frac{\partial v_y}{\partial x}+\frac{\partial v_x}{\partial y}\right)$$
$$+\frac{1}{R}\frac{\partial}{\partial \theta}\mu\left(\frac{\partial v_\theta}{\partial y}+\frac{\partial v_y}{\partial \theta}\right)+\frac{\partial}{\partial y}\mu\left\{2\frac{\partial v_y}{\partial y}-\frac{2}{3}\left[\frac{1}{R}\frac{\partial\left(Rv_x\right)}{\partial x}+\frac{1}{R}\frac{\partial v_\theta}{\partial \theta}+\frac{\partial v_y}{\partial y}\right]\right\}; \quad (9)$$

energy equation:

$$\rho_e c_p\left(v_x\frac{\partial T}{\partial x}+\frac{v_\theta}{R}\frac{\partial T}{\partial \theta}+v_y\frac{\partial T}{\partial y}\right)=\frac{1}{R}\frac{\partial}{\partial x}\left(\lambda R\frac{\partial T}{\partial x}\right)+\frac{1}{R}\frac{\partial}{\partial \theta}\left(\lambda\frac{\partial T}{R\partial \theta}\right)$$
$$+\frac{\partial}{\partial y}\left(\lambda\frac{\partial T}{\partial y}\right)+\frac{j^2}{\varkappa}; \quad (10)$$

where: v_x, v_θ, v_y – velocity vector components, p – pressure of the mixture of electrolyte and hydrogen, $\rho_e=(1-\beta)\rho_e^0$ – electrolyte equivalent density, $\rho_H=\beta\rho_H^0$ – hydrogen equivalent density, μ_e – dynamic coefficient of electrolyte viscosity, $\varkappa$ – electrolyte conductivity, j, η_H, k_H – current density, current efficiency of the hydrogen dissolution, electrochemical equivalent of hydrogen, T – temperature, c_p – specific heat capacity at constant pressure, R – radius of the surface of TE, $R'=\dfrac{\partial R}{\partial x}$.

The system of equations above (5)–(10) describes a steady three-dimensional flow of the mixture of electrolyte and hydrogen in the locally orthogonal curvilinear system of coordinates $x\theta y$ in the case of a lack of concentricity of the tool electrode and the WP.

If in the ECM process the TE and the WP is maintained, i.e., $\partial/\partial\theta\equiv 0$, then the flow of the mixture of electrolyte and hydrogen becomes an axisymmetric flow.

To include the effect of inertial forces in the two-phase medium flow, two classes of estimations referred to the velocity and pressure components have been considered [23]:

Estimation class I:

$$v_x=O\left(v_0\right), \quad v_\theta=O\left(v_0\right), \quad v_y=O\left(v_0\frac{h_0}{R_0}\right), \quad p=O\left(\frac{\mu v_0}{h_0}\frac{R_0}{h_0}\right). \quad (11)$$

Estimation class II:

$$v_x=O\left(v_0\frac{h_0}{R_0}\right), \quad v_\theta=O\left(v_0\right), \quad v_y=O\left(v_0\frac{h_0^2}{R_0^2}\right), \quad p=O\left(\frac{\mu v_0}{h_0}\right). \quad (12)$$

In dependencies (11) and (12) the respective symbols have been used: v_0 – means electrolyte flow rate, h_0 – means IEG thickness, R_0 – means radius of the area of the TE.

Introducing dependencies (11)–(12) to the system of equations (5)–(9) and disregarding small higher-order components, the simplified forms of motion equations have been established for both electrolyte mixture flow classes considered [26].

Flow class I:

flow continuity equations:

for electrolyte:

$$\frac{1}{R}\frac{\partial\left(\rho_e R v_x\right)}{\partial x}+\frac{\partial\left(\rho_e v_y\right)}{\partial y}=0; \tag{13}$$

for hydrogen:

$$\frac{1}{R}\frac{\partial\left(\rho_H R v_x\right)}{\partial x}+\frac{\partial\left(\rho_H v_y\right)}{\partial y}=j\eta_H k_H h^{-1}; \tag{14}$$

momentum equation:

$$\rho_e\left(v_x\frac{\partial v_x}{\partial x}+v_y\frac{\partial v_x}{\partial y}-v_\theta^2\frac{R'}{R}\right)=-\frac{\partial p}{\partial x}+\frac{\partial}{\partial y}\mu\left(\frac{\partial v_x}{\partial y}\right), \tag{15}$$

$$\rho_e\left(v_x\frac{\partial v_\theta}{\partial x}+v_y\frac{\partial v_\theta}{\partial y}+v_x v_\theta\frac{R'}{R}\right)=\frac{\partial}{\partial y}\mu\left(\frac{\partial v_\theta}{\partial y}\right), \tag{16}$$

$$0=-\frac{\partial p}{\partial y}; \tag{17}$$

energy equation:

$$v_x\frac{\partial T}{\partial x}+v_y\frac{\partial T}{\partial y}=\frac{\partial}{\partial y}\left(a\frac{\partial T}{\partial y}\right)+\frac{j^2}{\rho_e c_p \varkappa}; \tag{18}$$

where $a=\dfrac{\lambda}{\rho_e c_p}$ – thermal diffusivity.

Flow class II:

flow continuity equations:

for electrolyte:

$$\frac{1}{R}\frac{\partial\left(\rho_e R v_x\right)}{\partial x}+\frac{\partial\left(\rho_e v_y\right)}{\partial y}=0; \tag{19}$$

for hydrogen:

$$\frac{1}{R}\frac{\partial\left(\rho_H R v_x\right)}{\partial x}+\frac{\partial\left(\rho_H v_y\right)}{\partial y}=j\frac{\eta_H k_H}{h}; \tag{20}$$

momentum equation:

$$-\rho_e v_\theta^2\frac{R'}{R}=-\frac{\partial p}{\partial x}+\frac{\partial}{\partial y}\mu\left(\frac{\partial v_x}{\partial y}\right), \tag{21}$$

$$0 = \frac{\partial}{\partial y}\mu\left(\frac{\partial v_\theta}{\partial y}\right), \tag{22}$$

$$0 = -\frac{\partial p}{\partial y}; \tag{23}$$

energy equation:

$$v_x\frac{\partial T}{\partial x} + v_y\frac{\partial T}{\partial y} = \frac{\partial}{\partial y}\left(a\frac{\partial T}{\partial y}\right) + \frac{j^2}{\rho_e c_p \varkappa}. \tag{24}$$

The formulated two systems of equations (13)–(24) of axisymmetric, steady, and laminar flow of the mixture of electrolyte and hydrogen in the IEG allow the analysis of the effect of the inertial forces on the distributions of velocity and pressure, and thus, the distributions of temperature in the IEG.

2.3. Boundary conditions

The (13)–(24) solutions of equations should meet the boundary conditions for velocity and pressure components, respectively [23, 26]:

velocity components:

$$\begin{aligned} &v_x = v_y = 0 \quad \text{when} \quad y = 0 \quad \text{and} \quad v_x = 0, \quad v_y = 0 \quad \text{when} \quad y = h, \\ &v_\theta = 0 \quad \text{when} \quad y = 0 \quad \text{and} \quad v_\theta = \omega R(x) \quad \text{when} \quad y = h; \end{aligned} \tag{25}$$

pressure:

$$p = p_o \quad \text{for} \quad x = x_o; \tag{26}$$

for temperature:

$$\begin{aligned} &\text{on the walls:} \quad T = T_e \quad \text{for} \quad x \geqslant x_i \quad \text{and} \quad y = 0 \quad \text{and} \quad y = h, \\ &\text{on the inlet:} \quad T = T_i \quad \text{for} \quad x = x_i, \end{aligned} \tag{27}$$

where: p_o – pressure on the IEG outlet, x_i, x_o – IEG inlet and outlet coordinates, T_e – temperature of the electrodes, T_i – electrolyte temperature on the inlet.

2.4. Integrals of the equations of the electrolyte and hydrogen mixture flow

Introducing the characteristic dimensionless variables determined with the following formulas [26] to equations (13)–(24):

$$\begin{aligned} &\tilde{x} = \frac{x}{R_o}, \quad \tilde{y} = \frac{y}{h_o}, \quad \tilde{R} = \frac{R}{R_o}, \quad \tilde{\varrho}_e = \frac{\varrho_e}{\varrho_e^0}, \\ &\tilde{v}_x = \frac{v_x}{v_o}, \quad \tilde{v}_y = \frac{v_y}{v_o}\frac{R_o}{h_o}, \quad \tilde{v}_\theta = \frac{v_\theta}{v_o}, \quad \tilde{p} = \frac{p h_o}{\mu v_o}\frac{h_o}{R_o}, \end{aligned} \tag{28}$$

the continuity equation for electrolyte and momentum equations, describing a flow of the mixture of electrolyte and hydrogen, can be presented in the following form:

$$\frac{1}{\tilde{R}}\frac{\partial\left(\tilde{\rho}_e R\tilde{v}_x\right)}{\partial\tilde{x}}+\frac{\partial\left(\tilde{\rho}_e\tilde{v}_y\right)}{\partial\tilde{y}}=0, \tag{29}$$

$$\lambda\left(\tilde{v}_x\frac{\partial\tilde{v}_x}{\partial\tilde{x}}+v_y\frac{\partial\tilde{v}_x}{\partial\tilde{y}}-\tilde{v}_\theta^2\frac{\tilde{R}'}{\tilde{R}}\right)=-\frac{\partial\tilde{p}}{\partial\tilde{x}}+\frac{\partial^2\tilde{v}_x}{\partial\tilde{y}^2}, \tag{30}$$

$$\lambda\left(\tilde{v}_\theta\frac{\partial\tilde{v}_\theta}{\partial\tilde{x}}+v_y\frac{\partial\tilde{v}_\theta}{\partial\tilde{y}}-\tilde{v}_x\tilde{v}_\theta\frac{\tilde{R}'}{\tilde{R}}\right)=\frac{\partial^2\tilde{v}_\theta}{\partial\tilde{y}^2}, \tag{31}$$

$$0=-\frac{\partial\tilde{p}}{\partial\tilde{y}}. \tag{32}$$

The quantities with zero index are mean quantities in the flow area considered, $\lambda=\mathrm{Re}\dfrac{h_0}{R_0}$ – a modified Reynolds number.

In the equations of motion (30) and (31) the modified Reynolds number is the so-called small parameter of the system.

Thus its solution can be found in a form of power series for λ in a form of:

$$\tilde{v}_x=\sum_{i=0}^{\infty}\lambda^i\tilde{v}_x^i,\quad \tilde{v}_y=\sum_{i=0}^{\infty}\lambda^i\tilde{v}_y^i,\quad \tilde{v}_\theta=\sum_{i=0}^{\infty}\lambda^i\tilde{v}_\theta^i,\quad \tilde{p}=\sum_{i=0}^{\infty}\lambda^i\tilde{p}^i. \tag{33}$$

Substituting the series (33) to the equations of motion (30) and (31) and the flow continuity equation (29), ordering and grouping the terms for the same powers λ, limiting itself to the linear approximation and returning to the dimensional form, the following series of equations has been obtained [26]:

$$\frac{1}{R}\frac{\partial\left(\rho_e R v_x^0\right)}{\partial x}+\frac{\partial\left(\rho_e v_y^0\right)}{\partial y}=0, \tag{34}$$

$$\frac{1}{R}\frac{\partial\left(\rho_H R v_x^0\right)}{\partial x}+\frac{\partial\left(\rho_H v_y^0\right)}{\partial y}=j\frac{\eta_H k_H}{h}, \tag{35}$$

$$0=-\frac{\partial p^0}{\partial x}+\frac{\partial}{\partial y}\mu\left(\frac{\partial v_x^0}{\partial y}\right), \tag{36}$$

$$0=\frac{\partial}{\partial y}\mu\left(\frac{\partial v_\theta^0}{\partial y}\right), \tag{37}$$

$$\frac{1}{R}\frac{\partial\left(\rho_e R v_x^1\right)}{\partial x}+\frac{\partial\left(\rho_e v_y^1\right)}{\partial y}=0, \tag{38}$$

$$\rho_e \left[v_x^0 \frac{\partial v_x^0}{\partial x} + v_y^0 \frac{\partial v_x^0}{\partial y} - \left(v_\theta^0\right)^2 \frac{R'}{R} \right] = -\frac{\partial p^1}{\partial x} + \frac{\partial}{\partial y}\mu \left(\frac{\partial v_x^1}{\partial y} \right), \tag{39}$$

$$\rho_e \left(v_x^0 \frac{\partial v_\theta^0}{\partial x} + v_y^0 \frac{\partial v_\theta^0}{\partial y} - v_x^0 v_\theta^0 \frac{R'}{R} \right) = \frac{\partial}{\partial y}\mu \left(\frac{\partial v_\theta^1}{\partial y} \right). \tag{40}$$

Boundary conditions for the system of equations (34)–(40) now assume the form:

for velocity:

when $y = 0$ (on the surface of the TE):

$$v_x^0 = 0, \quad v_y^0 = 0, \quad v_\theta^0 = 0, \quad v_x^1 = 0, \quad v_y^1 = 0, \quad v_\theta^1 = 0; \tag{41}$$

for $y = h$ (on the surface of the WP):

$$v_x^0 = 0, \quad v_y^0 = 0, \quad v_\theta^0 = \omega R, \quad v_x^1 = 0, \quad v_y^1 = 0, \quad v_\theta^1 = 0; \tag{42}$$

for pressure:

$$p^0 = p_o\,, \quad p^1 = 0 \quad \text{when} \quad x = x_o\,. \tag{43}$$

Solving the sequence of equations received using the boundary conditions (41)–(43) the distribution of velocity and pressure in the IEG have been respectively received for:

Flow class I:

$$v_x = \frac{3Q}{\pi R h^3}\left(hy - y^2\right) + \frac{\rho}{\mu}\left(\frac{27}{140}\frac{Q^2R'}{\pi^2R^3h^2} + \frac{3}{20}\omega^2RR'\right)\left(y^2 - hy\right)$$
$$+ \frac{\rho}{\mu}\left[\frac{3}{20}\frac{Q^2R'}{\pi^2R^3h^6}\left(6hy^5 - 5h^2y^4 - 2y^6 + h^5y\right) - \frac{1}{12}\frac{\omega^2RR'}{h^2}\left(y^4 - h^3y\right)\right], \tag{44}$$

$$v_\theta = \omega R\frac{y}{h} + \frac{1}{20}\frac{\rho}{\mu}\left[\frac{2Q\omega R'}{\pi R h^4}\left(5hy^4 - 3y^5 - 2h^4y\right)\right], \tag{45}$$

$$v_y = \frac{V}{h^3}\left(3hy^2 - 2y^3\right) - \frac{1}{\rho_e R}\frac{\partial}{\partial x}\left\{\frac{\rho}{\mu}\left(\frac{27}{140}\frac{Q^2R'}{\pi^2R^3h^2} + \frac{3}{20}\omega^2RR'\right)\left(y^2 - hy\right)\right.$$
$$\left. + \frac{\rho}{\mu}\left[\frac{3}{20}\frac{Q^2R'}{\pi^2R^3h^6}\left(6hy^5 - 5h^2y^4 - 2y^6 + h^5y\right) - \frac{1}{12}\frac{\omega^2RR'}{h^2}\left(y^4 - h^3y\right)\right]\right\}, \tag{46}$$

$$p(x) = -\frac{6\mu Q}{\pi h^3}\left(A_x - A_z\right) + \frac{27}{70}\frac{\rho Q^2}{\pi^2h^2}\left(B_x - B_z\right) + \frac{3}{20}\rho\omega^2\left(R^2 - R_z^2\right) + p_a\,, \tag{47}$$

where:

$$v_x^0 = \frac{3Q}{\pi R h^3}\left(hy - y^2\right), \tag{48}$$

$$v_x^1 = \frac{\rho}{\mu}\left(\frac{27}{140}\frac{Q^2R'}{\pi^2R^3h^2} + \frac{3}{20}\omega^2RR'\right)\left(y^2 - hy\right) + \frac{\rho}{\mu}\left[\frac{3}{20}\frac{Q^2R'}{\pi^2R^3h^6}\left(6hy^5 - 5h^2y^4 - 2y^6 + h^5y\right) - \frac{1}{12}\frac{\omega^2RR'}{h^2}\left(y^4 - h^3y\right)\right], \quad (49)$$

$$v_\theta^0 = \omega R\frac{y}{h}, \quad (50)$$

$$v_\theta^1 = \frac{1}{20}\frac{\rho}{\mu}\left[\frac{2Q\omega R'}{\pi Rh^4}\left(5hy^4 - 3y^5 - 2h^4y\right)\right], \quad (51)$$

$$v_y^0 = 0, \quad (52)$$

$$v_y^1 = -\frac{1}{\rho_e R}\frac{\partial}{\partial x}\left\{\frac{\rho}{\mu}\left(\frac{27}{140}\frac{Q^2R'}{\pi^2R^3h^2} + \frac{3}{20}\omega^2RR'\right)\left(y^2 - hy\right) - \frac{\rho}{\mu}\left[\frac{3}{20}\frac{Q^2R'}{\pi^2R^3h^6}\left(6hy^5 - 5h^2y^4 - 2y^6 + h^5y\right) - \frac{1}{12}\frac{\omega^2RR'}{h^2}\left(y^4 - h^3y\right)\right]\right\}, \quad (53)$$

$$p^0(x) = -\frac{6\mu Q}{\pi h^3}\left(A_x - A_z\right) + p_a, \quad (54)$$

$$p^1(x) = \frac{27}{70}\frac{\rho Q^2}{\pi^2h^2}\left(B_x - B_z\right) + \frac{3}{20}\rho\omega^2\left(R^2 - R_z^2\right), \quad (55)$$

where:

$$A_x = \int\frac{\mathrm{d}x}{R}, \quad B_x = -\frac{1}{2R^2}, \quad C_x = \int\frac{\mathrm{d}x}{R^2}\mathrm{d}x,$$

$$D_x = \int\rho_e RR'\,\mathrm{d}x, \quad A_z = A\left(x_z\right), \quad B_z = B\left(x_z\right).$$

Flow class II:

$$v_x = \frac{3Q}{\pi Rh^3}\left(hy - y^2\right) + \frac{\rho}{\mu}\left(\frac{3}{20}\omega^2RR'\right)\left(y^2 - hy\right) + \frac{\rho}{\mu}\left[\frac{1}{12}\frac{\omega^2RR'}{h^2}\left(y^4 - h^3y\right)\right], \quad (56)$$

$$v_\theta = \omega R\frac{y}{h}, \quad (57)$$

$$v_y = -\frac{1}{\rho_e R}\frac{\partial}{\partial x}\left\{\frac{\rho}{\mu}\left(\frac{3}{20}\omega^2RR'\right)\left(y^2 - hy\right) + \frac{\rho}{\mu}\left[-\frac{1}{12}\frac{\omega^2RR'}{h^2}\left(y^4 - h^3y\right)\right]\right\}, \quad (58)$$

$$p(x) = -\frac{6\mu Q}{\pi h^3}\left(A_x - A_z\right) + \frac{3}{20}\rho\omega^2\left(R^2 - R_z^2\right) + p_a, \quad (59)$$

where: $A_x = \int\frac{\mathrm{d}x}{R}$, $A_z = A\left(x_z\right)$.

Knowing the velocity distribution in the cross-sections of the IEG, using the equation of (24) and the applicable boundary conditions (27), the temperature distributions have been numerically determined with the finite difference method to solve the shape evolution equation (2).

For the numerical solution of the shape evolution equation of the WP (2), the Euler method has been applied [26].

Time t has been presented on the time grid in a form of a set of points:

$$t^n = t^0 + n\Delta t\,, \tag{60}$$

where: $n = 0,\ 1,\ 2,\ 3,\ \ldots,\ N$.

The TE and the WP have been discretized in a global cylindrical coordinate system applying, respectively, the axisymmetry for rotational body, namely assuming that:

$$R_i = R_0 + i\Delta R, \tag{61}$$

where: $i = 0,\ 1,\ 2,\ 3,\ \ldots,\ I$, $\Delta R = \dfrac{R_z - R_w}{I}$.

Substituting the derivatives in equation (2) with simple differentia terms [19] and index A of the selected point on anode with index I, the following sequence of algebraic equations has been received:

– when $i = 0$:

$$Z_i^{n+1} = Z_i^n - \left[k_V j_A \sqrt{1 + \left(\frac{Z_i^n - Z_{i+1}^n}{\Delta R}\right)^2}\right]\Delta t, \tag{62}$$

– when: $0 < i < I$

$$Z_i^{n+1} = Z_i^n - \left[k_V j_A \sqrt{1 + \left(\frac{Z_{i-1}^n - Z_{i+1}^n}{2\Delta R}\right)^2}\right]\Delta t, \tag{63}$$

– when: $i = I$

$$Z_i^{n+1} = Z_i^n - \left[k_V j_A \sqrt{1 + \left(\frac{Z_{i-1}^n - Z_i^n}{\Delta R}\right)^2}\right]\Delta t. \tag{64}$$

Differential equations (62–64) allow us to determine new coordinate points of anode (WP) in the global Cartesian coordinate system ZR in successive Δt time iterations (Fig. 2).

However, one shall note that to determine new coordinates of the points of anode (WP) one must calculate indispensable parameters to determine current density j_i, along the IEG: medium flow velocity v_x, v_θ, v_y, pressure p, concentration of gas phase β and temperature T.

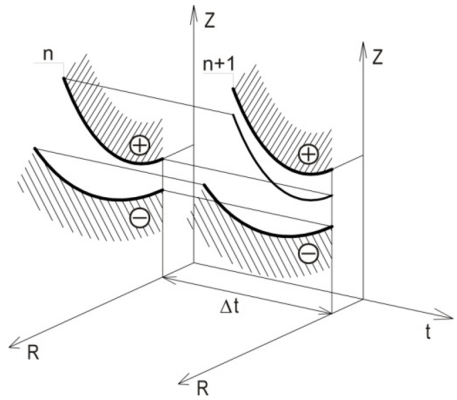

Fig. 2. Effect of ECM process time on shape evolution WP

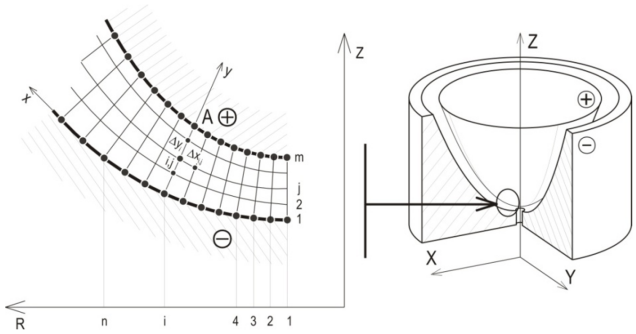

Fig. 3. Numerical grid of the electrolyte flow area

Time t for the method of solving the shape evolution equation for the WP discussed acts as the parameter – a sequence of tasks appears with the so-called "frozen" IEG thickness distribution for given moment t^n.

A discrete form of the equation has been obtained through substituting the derivatives in equation (24) with differential terms [26], from which in turn the value of the temperature in successive mesh nodes has been calculated (Fig. 3):

$$T_{i,j}^{k} = \frac{T_{i-1,j} + \gamma_1 \left(T_{i-1,j+1} - 2T_{i-1,j} + T_{i-1,j-1} + T_{i,j+1}^{k-1} + T_{i,j-1} \right)}{1 + 2\gamma_1} - \frac{\dfrac{v_{y\,i,j}}{v_{x\,i,j}} \dfrac{\Delta x_{i,j}}{\Delta y_i} \left(T_{i-1,j}^{k-1} - T_{i-1,j-1} \right) + \gamma_2}{1 + 2\gamma_1}, \tag{65}$$

where:

$$\gamma_1 = \frac{a_{i,j} \Delta x_{i,j}}{2 v_{x\,i,j} \Delta y_j^2}, \qquad \gamma_2 = \frac{j_i^2}{\rho_i c_p \varkappa_{i,j} v_{x\,i,j}}, \tag{66}$$

index k – successive iteration number.

The thermal diffusivity coefficient in the laminar flow conditions is determined with the following formula [17, 26]:

$$a_{i,j} = \frac{\lambda}{\rho c_p}, \qquad \lambda = \lambda_0(1-\beta), \tag{67}$$

where: λ – thermal conductivity, λ_0 – thermal conductivity at T_0.

Defined with dependence (65), the approximate differential equation was solved with the iteration method. The iteration calculations are repeated until the calculation accuracy condition is met. The knowledge of the physical fields of the electrolyte flow has facilitated an effective determination of the WP shape (anode).

The ECM computer simulation algorithm for the shaped surfaces is given in Fig. 4.

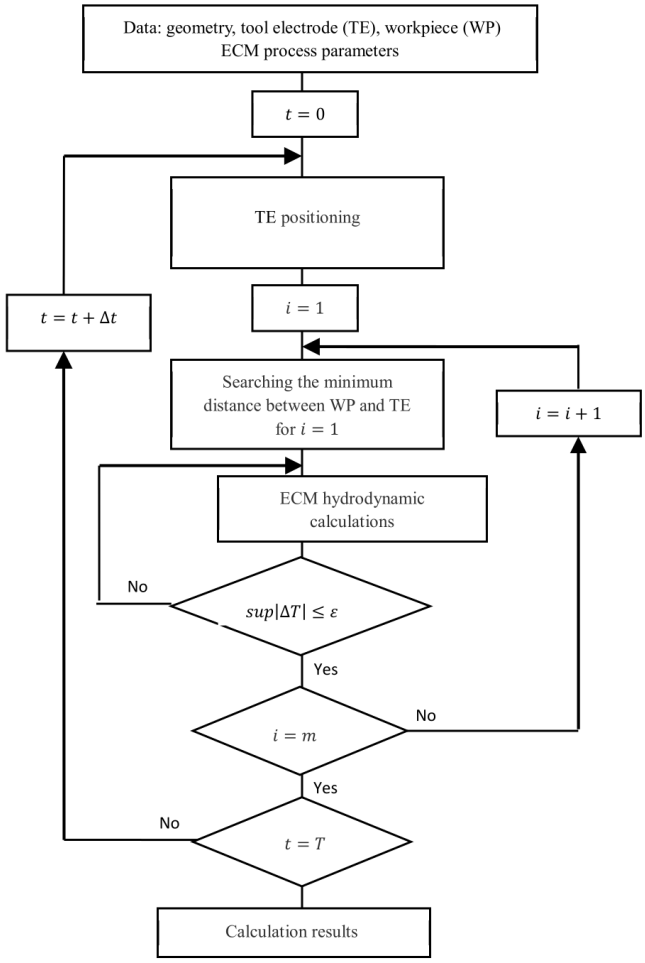

Fig. 4. ECM process simulation algorithm (markings: i, m – current and the last point of the curve describing the WP)

3. Computer simulation results

The geometric features of the WP and the TE are presented in Fig. 5.

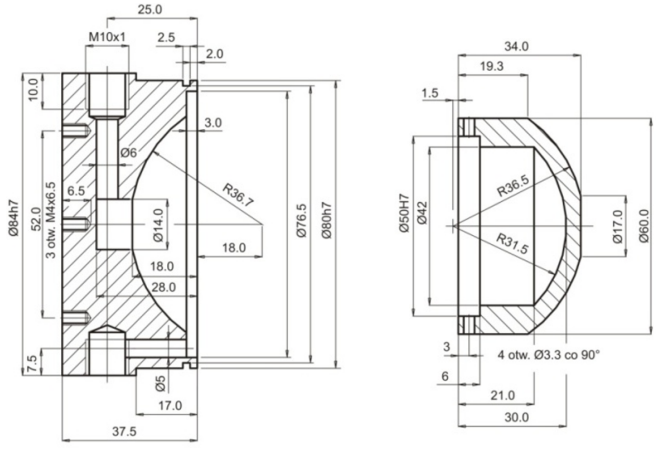

(a) (b)

Fig. 5. Geometric features: TE and WP

To enable computer simulation of ECM process of rotary surfaces, an application in Delphi language was developed, based on the mathematical model of rotary surface ECM process and the algorithm presented above.

For the calculations, the following key machining parameters have been considered (Table 1).

Table 1. Machining parameters

Parameters		Specifications
Inlet radius	R_i	17 mm
Outlet radius	R_o	30 mm
Initial gap	h	0.2 mm
Feed rate of the TE	V_f	1 mm min^{-1}
Working voltage	U	15 V
Volumetric flow rate	Q	3 dm^{3}min^{-1}
Outlet pressure	p_o	0.1 MPa
Machining time	t	200 s
Workpiece material	WP	alloy tool steel 2312
Electrochemical machinability	k_V	$= 1.59(1 - \exp(2.56 - 0.112j)$ mm^3(A$_{\min}$)$^{-1}$ current density j is in A cm^{-2}
Electrolyte		15% water solution of $NaNO_3$

The calculations were carried out for the values of rotational speed WP (n = 1000 rpm) assuming a passivating electrolyte and constant machining time.

The calculations results V_x, p, T, j, β, h are graphically presented in Figs 6–11.

In Figs 6–11, we showed the influence of inertia forces on the physical parameters of ECM process. The distribution of ECM processing parameters (i.e.: electrolyte flow velocity, pressure, temperature, flow coefficients, gas phase concentration and gap thickness changes), for the so-called Reynolds approximate,

(RA – Reynolds approximation, ECF – Effect of centrifugal forces,
ELCF – Effect of longitudinal and centrifugal forces)

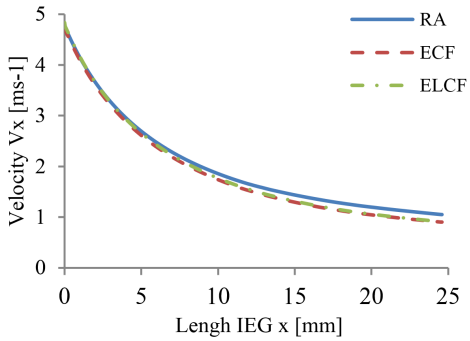

Fig. 6. Velocity distribution v_x

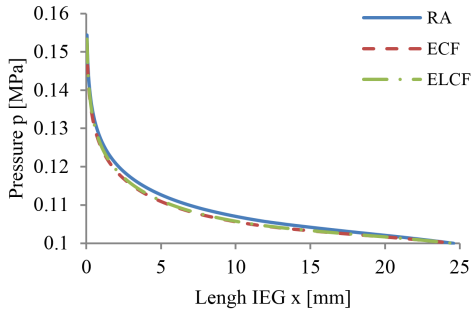

Fig. 7. Pressure distribution p

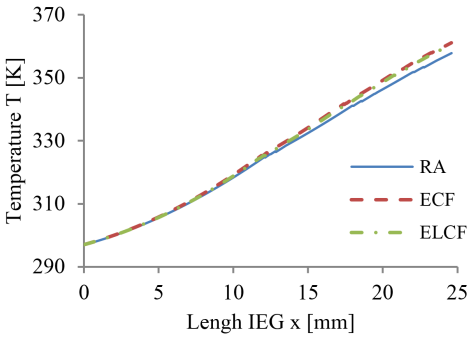

Fig. 8. Temperature distribution T

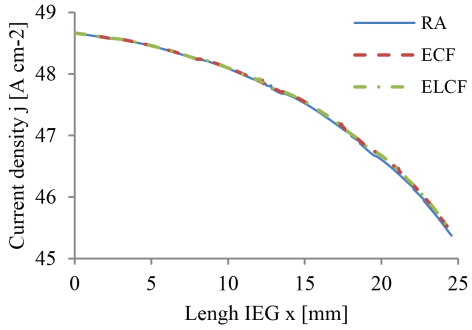

Fig. 9. Current density distribution j

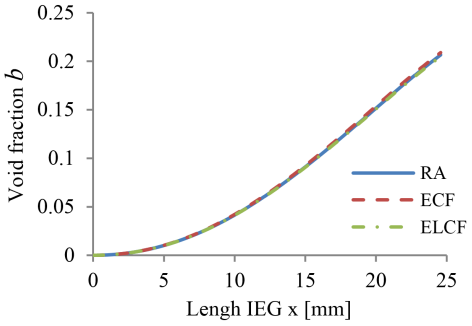

Fig. 10. Void fraction distribution β

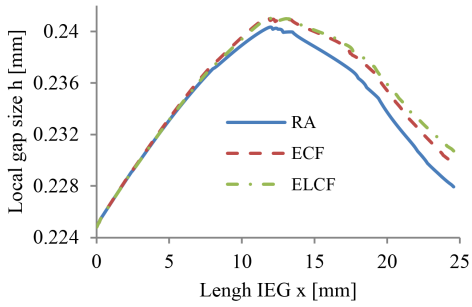

Fig. 11. Local gap size distribution h

which ignores the influence of inertia forces on electrolyte flow, was demonstrated. Based on the obtained distribution of machining parameters, characteristic for the approximate Reynolds value, the search for results is intended for the second class of CIF flow (influence of centrifugal inertia forces) and for the approximation of the first class LCIF flow (effect of longitudinal and centrifugal inertia forces).

The influence of inertia forces results from the fact that the equation of momentum includes the electrolyte flow in the inter-electrode gap of the corresponding members characteristic for class I and class II flows.

The analysis of the influence of inertial flow forces of electrolyte in the gap (IEG) on the ECM treatment parameters allows one to formulate the following conclusions:

- the solution, based on the approximate characteristic for the second class of CIF flows, allows the analysis of centrifugal inertia forces. The effect of centrifugal inertia forces caused by anode rotation for given machining parameters significantly affects the distribution of speed, pressure, temperature, and thickness values of the electrode gap. The impact of inertia forces caused by anode rotation on the distribution of current density and gas phase concentration is negligible. It is worth to notice that the effect of inertial forces caused by rotation depends on the WP rotation speed. Higher rotational speed may lead to interruption of the electrolyte flow in the gap due to vacuum appearing along the gap length.
- a solution based on the use of class 1 flows, i.e., the approximation, which takes into account the effect of longitudinal and centrifugal inertial forces (CIF), results from the analysis of nonlinear equations of electrolyte flow movement in the (IEG) gap. The analytical solution of these equations requires the use of approximate methods which lead to complicated formulas determining the velocity and pressure flow field. When comparing the effect of longitudinal and centrifugal inertia forces on the electrolyte flow and thus on the physical parameters of ECM treatment, it should be noted that in relation to the Reynolds approximation this effect is similar to the results characteristic for the second class of flows, which only takes into account the centrifugal force resulting from the set WP speed. It is noteworthy that the influence of the longitudinal force of inertia of the flow (radial) depends on the value of the given stream by volume, and the value of this stream determines the nature of the electrolyte flow, i.e., laminar or turbulent. In terms of laminar flow, this impact should be considered as insignificant, compared to solving the problem based on class II flows.

All things considered, it seems that within the range of machining parameters adopted for the calculations, the solution described in class II flows is sufficient to analyze the ECM process of curvilinear rotary surfaces.

The mathematical model of the ECM process presented in the article was experimentally verified on the stand presented in Fig. 12 [26]. One can distinguish here a body consisting of plates (1) mounted on four guides (2) and drive systems

(3), (4) implementing the given process kinematics. A processing cell is attached to the body in its central part. The processing cell consists of a working electrode (5) (Fig. 5a) and a workpiece (Fig. 5b) mounted in a sealing cover (6) made of electrically non-conductive material.

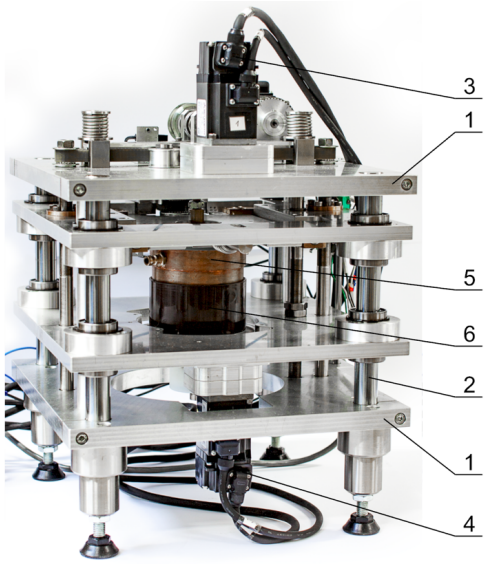

Fig. 12. Test stand: 1 – body plate, 2 – guide, 3 – DC motors (servo) – feed movement V_f, 4 – DC motors (servo) – rotary movement, 5 – TE, 6 – WP cover

To assess the accuracy of the proposed mathematical model of the ECM process, the distribution of the shape deviation (δ) of the WP obtained from mathematical calculations and the shape of the WP obtained after processing on the test stand were adopted. The deviation measurement results did not exceed the value of $\delta_{max} = 0.05$ mm.

4. Conclusions

The design of ECM technology for machine parts and tools requires using information technology, particularly when we want to design the working electrode both quickly and accurately. The application of computer design for ECM process leads to computer simulations based on the analysis and mathematical modeling of the ECM process.

This work is an attempt to analyze the influence of electrolyte flow inertia forces on physical parameters of the electrochemical machining process of curvilinear rotating surfaces, such as: average speed, pressure, average temperature, current density, gas phase concentration, and local gap thickness distribution after a given machining time.

Two classes of flows were considered, differing in the order of magnitude of individual components of the flow velocity, formulating the equations of electrolyte movement in the inter-electrode gap, respectively. The equations describing the second class of flows are a special case of the equations representing the first class of flows. Flow class I allows the analysis of the influence of longitudinal and centrifugal inertia forces on the electrolyte flow. Class II flow allows the analysis of the impact of centrifugal inertia forces on the electrolyte flow and, at the same time, on the physical parameters of ECM treatment.

The equations describing the first class of flows were solved by the method of small parameter (method of perturbation) determining the field of velocity and pressure in the inter-electrode gap. The solution of class II flows was a special case of the solution of class I flows.

The obtained complex analytical functions of velocity and pressure distributions were used to numerically determine the temperature distributions and then the WP shape, with the help of the anode shape evolution equation known in theory.

The equation of shape evolution was solved using the so-called time steps from the method of successive approximations.

The equation resulting from the principle of conservation of energy was solved by the finite difference method.

It should be noted that, in order to investigate the impact of electrolyte flow and inertia forces on the physical parameters of ECM treatment, it was necessary to solve complex non-linear systems of differential equations resulting from the principles of mass, momentum and energy conservation for the electrolyte and hydrogen mixture flow in the inter-electrode gap.

References

[1] G. Chrysslouris, M. Wollowitz, and N.P. Sun. Electrochemical hole making. *Annals CIRP*, 33(1):99–104, 1984. doi: 10.1016/S0007-8506(07)61388-2.

[2] M. Datta and L.T. Romankiw. Application of chemical and electrochemical micromachining in the electronics industry. *Journal of Electrochemical Society*, 136(6):285–292, 1989. doi: 10.1149/1.2097055.

[3] A. Ruszaj. Electrochemical machining – state of the art and direction of development. *Mechanik*, 90(12):1102–1109, 2017. doi: 10.17814/mechanik.2017.12.188.

[4] A. Ruszaj, J. Gawlik, and S. Skoczypiec. Electrochemical machining – special equipment and applications in aircraft industry. *Management and Production Engineering Review*, 7(2):34–41, 2016. doi: 10.1515/mper-2016-0015.

[5] K.P. Rajurkar, M.M. Sundaram,and A.P. Malshe. Review of electrochemical and electro discharge machining. *Procedia CIRP*, 6:13–26, 2013. doi: 10.1016/j.procir.2013.03.002.

[6] J. Bannard. Electrochemical machining. *Journal of Applied Electrochemistry*, 7:1–29, 1977. doi: 10.1007/BF00615526.

[7] J.A. McGeough. *Principles of Electrochemical Machining*. Chapman and Hall, London, 1974.

[8] J.A. McGeough and H. Rasmussen. Theoretical analysis of the electroforming process. *Journal Mechanical Engineering Science*, 23(3):113–120, 1981. doi: 10.1243/JMES_JOUR_1981_023_024_02.

[9] H.S.J. Altena. *Precision ECM by process characteristic modelling*. Ph.D. Thesis, Glasgow Caledonian University. 2000.

[10] A. Budzyński and S. Seroka. Studies of unidirectional longitudinal electrochemical honing. *Conference Materials EM-82*, Bydgoszcz, Poland, pages 152–161, 1982. (in Polish).

[11] L. Dąbrowski. *Basics of Computer Simulation of Electrochemical Forming*. Scientific Works, Mechanics 154, Publisher of Warsaw University of Technology. 1992. (in Polish).

[12] J. Kozak and M. Zybura-Skrabalak. Some problems of surface roughness in electrochemical machining. *Procedia CIRP*, 42:101–106, 2016. doi: 10.1016/j.procir.2016.02.198.

[13] K. Łubkowski, L. Dąbrowski, J. Kozak, and M. Rozenek. Electrochemical machine tools for surface smoothing and deburring. *Conference Materials EM-90*, Bydgoszcz, Poland, pages 78–86, 1990. (in Polish).

[14] X. Wang, H. Li, and S. Niu. Simulation and experimental research into combined electrochemical milling and electrochemical grinding machining of Ti40 titanium alloy. *International Journal Electrochemical Science*, 15:11150–11167, 2020. doi: 10.20964/2020.11.09.

[15] M. Singh and S. Singh. Electrochemical discharge machining: A review on preceding and perspective research. *Proceedings of the Institution of Mechanical Engineers, Part B: Journal of Engineering Manufacture*, 233(5):1425–1449, 2019. doi: 10.1177/0954405418798865.

[16] J.F. Wilson. *Practice and Theory of Electrochemical Machining*. Wiley, New York, 1971.

[17] J. Kozak. Mathematical models for computer simulation of electrochemical machining processes. *Journal of Materials Processing Technology*, 76(1-3):170–175, 1998. doi: 10.1016/S0924-0136(97)00333-6.

[18] J. Sawicki. ECM machining of curvilinear rotary surfaces by a shaping tool electrode performing composite motion. *Advances in Manufacturing Science and Technology*, 34(2):79–92, 2010.

[19] A.D. Davydov, V.M. Volgin, and V.V. Lyubimov. Electrochemical machining of metals: fundamentals of electrochemical shaping. *Russian Journal of Electrochemistry*, 40(12):1230–1265, 2004. doi: 10.1007/s11175-005-0002-6.

[20] J. Sawicki and T. Paczkowski. Effect of the hydrodynamic conditions of electrolyte flow on critical states in electrochemical machining. *EPJ Web of Conferences*, 92:02078, 2015. doi: 10.1051/epjconf/20159202078.

[21] C.F. Noble. *Studies in Electrochemical Machining*. PhD Thesis. University of Manchester, UK, 1976.

[22] H. Demitras, O. Yilmaz, and B. Kanber. Controlling short circuiting, oxide layer and cavitation problems in electrochemical machining of freeform surfaces. *Journal of Materials Processing Technology*, 262:585–596, 2018. doi: 10.1016/j.jmatprotec.2018.07.029.

[23] T. Paczkowski and J. Sawicki. Electrochemical machining of curvilinear surfaces. *Machining Science and Technology*, 12(1):33–52, 2008. doi: 10.1080/10910340701881433.

[24] T. Paczkowski and J. Zdrojewski. The mechanism of ECM technology design for curvilinear surfaces. *Procedia CIRP*, 42:356–361, 2016. doi: 10.1016/j.procir.2016.02.195.

[25] J. Sawicki. ECM machining of curvilinear rotary surfaces. *Journal of Polish CIMAC*. 5(3):88–98, 2010.

[26] J. Sawicki. *Analysis and Modeling of Electrochemical Machining of Curvilinear Rotary Surfaces*. University Publisher. UTP University of Science and Technology, Poznan, Poland, 2013.

[27] E.I. Filatov. The numerical simulation of the unsteady ECM process. *Journal of Materials Processing Technology*, 109(3):327–332, 2001. doi: 10.1016/S0924-0136(00)00817-7.

[28] C. Zhang, Z. Xu, Y. Hang, and J. Xing. Effect of solution conductivity on tool electrode wear in electrochemical discharge drilling of nickel-based alloy. *The International Journal of Advanced Manufacturing Technology*, 103:743–756, 2019. doi: 10.1007/s00170-019-03492-w.

[29] M. Chai, Z. Li, X. Song, J. Ren, and Q. Cui. Optimization and simulation of electrochemical machining of cooling holes on high temperature nickel-based alloy. *International Journal Electrochemical Science*, 16:210912, 2021. doi: 10.20964/2021.09.35.

[30] D. Mi and W. Natsu. Proposal of ECM method for holes with complex internal features by controlling conductive area ratio along tool electrode. *Precision Engineering*, 42:179–186, 2015. doi: 10.1016/j.precisioneng.2015.04.015.

[31] D. Zhu, R. Zhang, and C. Liu. Flow field improvement by optimizing turning profile at electrolyte inlet in electrochemical machining. *International Journal of Precision Engineering and Manufacturing*, 18(1):15–22, 2017. doi: 10.1007/s12541-017-0002-y.

[32] J. Kozak. *Surface Shaping Contactless Electrochemical Machining*. Scientific Works, Mechanics 41, Publisher of Warsaw University of Technology. 1976. (in Polish).

[33] Łubkowski K. *Critical States in Electrochemical Machining*. Scientific Works, Mechanics 163, Publisher of Warsaw University of Technology, 1996. (in Polish).